Forces on a Rayleigh Particle in the Cover Region of a Planar Waveguide

L. N. Ng, B. J. Luff, M. N. Zervas, *Member, IEEE*, and J. S. Wilkinson

***Abstract*—We report on the optimization of a waveguide structure for the maximization of the radiation forces exerted on a Rayleigh particle in the cover region. The two main radiation forces involved are the transverse gradient force which attracts a particle into the waveguide and the combined scattering and dissipative forces which drive the particle forward along the channel. The dependence of these forces on parameters including the incident wavelength, the surrounding medium embedding the particles, and the polarizability of the particles is discussed. Both dielectric and metallic gold spheres of radius 10 nm are considered in the model. Special emphasis is devoted to the maximization of the transverse gradient force due to the optical intensity gradient at the waveguide surface, and the wavelength dependence of the polarizability of gold nanoparticles.**

***Index Terms*—Chemical sensor, optical forces, optical planar waveguide, optical trapping, Rayleigh particles.**

I. Introduction

IT is well known that the foremost requirement to achieve optical trapping is to create a region of strong intensity gradient. Many researchers have achieved this by exploiting the intensity gradient from a tightly focused Gaussian beam [1]–[6]. The beam must be focused to a small spot as this ensures rapid divergence, producing a strong intensity gradient in the axial direction [7], [8]. This is known as a single beam Gaussian trap or optical tweezer [8]. Since 1970 when Ashkin [1] observed that Mie dielectric particles can be trapped and manipulated using a focused Gaussian beam, much effort has been devoted to exploring new techniques for trapping as well as manipulating particles in the Rayleigh and atomic regimes. For instance, Svoboda and Block demonstrated the trapping of Rayleigh gold spheres with a radius of 18 nm using a Gaussian trap [5]. Of particular interest is the use of the evanescent field as the propagating wave. This idea was first proposed by Cook and Hall for use in an atomic mirror in 1980 [9]. By tuning and detuning the frequency relative to the resonant frequency, an atom can either be attracted into or expelled from the region of high intensity [10]. Subsequently, the manipulation of Mie dielectric and 0.5 μm gold particles in the evanescent region of a prism [11] and channel waveguide [12] were reported by Kawata and coworkers. Following that, a nanometric optical tweezer was proposed by Novotny, Bian, and Xie, with the intensity gradient generated by the strong evanescent field around a 5-nm radius metal tip [13]. More recently, Taguchi and coworkers reported the levitation of polystyrene particles and yeast cells against gravity using the evanescent field at a tapered spherical polished end of a fiber [14].

Optical trapping offers a powerful, nonmechanical, nondestructive, and highly precise technique which finds extensive application particularly in the fields of cell sorting [15]–[17], cloud physics, aerosol science, and light scattering [18]. For instance, trapping of a particle may help improve accuracy in the recording and analysis of data as in the case of observing condensation or evaporation [18]. In recent years, growing interest has developed in using an optical trap as a probe for optical near-field microscopy (SNOM) to scan the surface of a sample. This idea was originally proposed by Kawata in 1994 [19]. A recent report on SNOM [20] has shown that image enhancement can be improved by as much as a factor of two thereby making it a valuable tool for carrying out sensitive measurements particularly on nanostructures.

Much of the theoretical work which has been reported to date mainly describes particles in the Mie regime. Analysis based on a Gaussian trap using both a geometrical ray approach [1], [7], [21] and a full EM model are well established [22], [23]. The latter has also been used to calculate forces in the evanescent field [24]. For particles in this regime, the origin of radiation forces can be explained by the reflection and refraction of light in the particle due to a momentum transfer between incident photons and the particle. In the Rayleigh regime, however, light induces a dipole in the particle which oscillates and reemits secondary radiation. In both cases, the total force can be decomposed into two main components: 1) the scattering and dissipative forces which act in the direction of wave propagation and 2) the gradient force which is proportional to the intensity gradient and acts in the direction toward or away from a high intensity region depending on the polarizability of a particle. To date, published work relating to forces exerted on Rayleigh particles have been presented mainly to handle configurations including a Gaussian standing wave [25], a focused Gaussian beam [26], and an evanescent field [27], [28] on an infinite slab structure.

The main contribution of this paper is the derivation of a normalized transcendental equation which can be used to optimize a planar waveguide with respect to parameters including thickness of the waveguide, incident wavelength, and the refractive indexes of the cover, guide and substrate, such

Manuscript received September 29, 1998; revised November 18, 1999. The Optoelectronics Research Centre is an Interdisciplinary Research Centre supported by the U.K. Engineering and Physical Sciences Research Council.

L. N. Ng, M. N. Zervas, and J. S. Wilkinson are with the Optoelectronics Research Centre, University of Southampton, Southampton SO17 1BJ, U.K.

B. J. Luff is with Bookham Technology, Abingdon, Oxfordshire OX14 4RY, U.K.

Publisher Item Identifier S 0733-8724(00)02185-X.

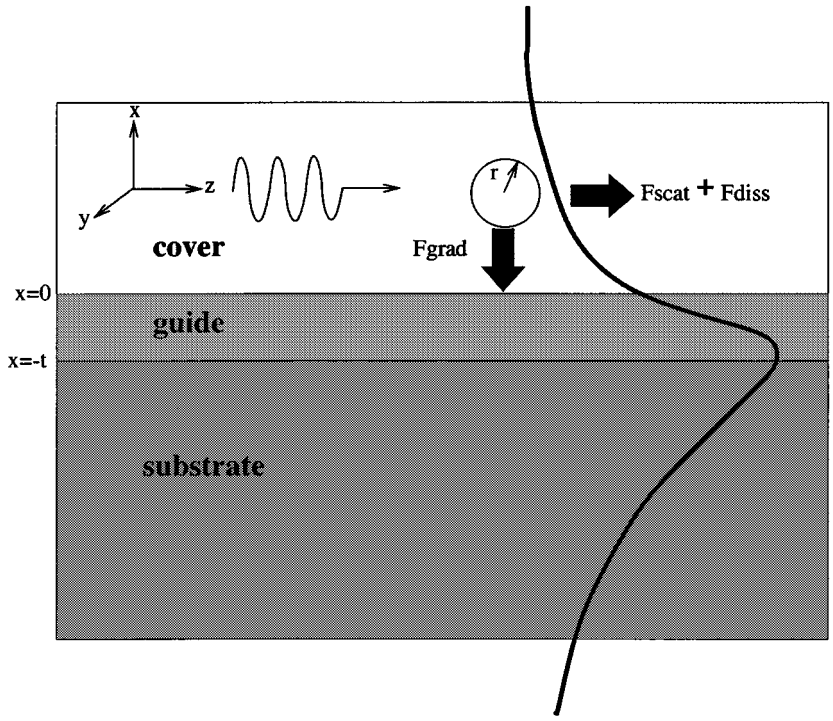

Fig. 1. Schematic representation of an asymmetric planar waveguide. Radiation forces acting on a sphere of radius r are decomposed into gradient force in the transverse direction and a forward force in the direction of wave propagation.

that a Rayleigh particle can be trapped in the transverse direction and driven in the forward direction by maximum radiation forces. The motivation for this work is to provide optimized waveguide designs where the strength of the trapping force is maximized thereby reducing the probability that particles escape the trap due to Brownian motion and other spurious influences. For simplicity, only the transverse electric (TE) polarization is considered; although a similar procedure could be applied to the transverse magnetic (TM) polarization, it is expected that little more physical insight would result. For comparison purposes, the metallic and dielectric spheres used throughout this paper are of radius $r = 10$nm, and all calculations and derivations are based on MKS units. Maximizing the gradient force can be achieved by maximizing both the intensity gradient in the cover region and the polarizability of a particle. Consideration of these two factors in relation to the gradient force provides results which will be useful for the manipulation of particles on planar waveguides with potential interest in particle sorting at surfaces and for their interrogation using evanescent field sensing techniques. In particular, colloidal metallic nanoparticles which exhibit resonance in the visible region are of great interest in the preparation of surfaces for surface-enhanced Raman spectroscopy [29].

In Section II, optimization of a waveguide to maximize the intensity gradient in the cover region, which leads to a maximum transverse gradient force, is derived in detail. Comparison is then made against a set of practical waveguide indexes. In Section III, the transverse and axial forces on a dielectric and a gold nanoparticle in the evanescent fields are discussed with particular emphasis on the wavelength-dependent polarizability of the latter. Finally, conclusions and future prospects are outlined in Section IV.

II. Optimizing the Intensity Gradient and Intensity in the Cover

For the purpose of completeness, we begin the derivation from the well-known dispersion equations of a slab waveguide. The waveguide configuration considered here is as illustrated in Fig. 1 where a particle interacts with the field in the cover region. In our case, the direction of wave propagation is taken as the $+z$ direction and only the TE mode is considered. Refractive indexes of the cover, guide and substrate regions, respectively, are designated as n_c, n_g, and n_s and the waveguide thickness is t. For the most common practical case of an asymmetrical waveguide where $n_s > n_c$, most of the power is confined in the guide and the substrate. This results in a very small proportion of the wave propagating in the cover region. A particle in this region would then experience a very small intensity gradient and hence a weak force, rendering optimization of the intensity gradient very important for practical application. The distribution of evanescent power in the cover region is also strongly influenced by waveguide thickness. It is convenient for analysis to normalize the thickness to the incident wavelength, so we define $t_{\mathrm{norm}} = t/\lambda$.

All the physical parameters of the waveguide, and the wavelength of light employed, have a direct effect on the magnitude of the gradient force. For this reason, optimization of the intensity gradient with respect to these parameters is essential and is discussed in Section II-B after expressions for normalized waveguide parameters corresponding to the structure are presented.

A. Normalized Waveguide Parameters

The dispersion relation, also known as the characteristic equation, of a TE mode for a planar waveguide structure is well known and is given here in a form consistent with the analysis by Parriaux *et al.* [30], [31], as

$$2\pi t_{\text{norm}}\sqrt{n_g^2 - n_{\text{eff}}^2} - \tan^{-1} X_s - \tan^{-1} X_c - m\pi = 0 \quad (1)$$

where $m = 0, 1, 2\ldots$ denotes the mth order of a mode while normalized parameters X_s and X_c are defined as

$$X_s = \sqrt{\frac{n_{\text{eff}}^2 - n_s^2}{n_g^2 - n_{\text{eff}}^2}} \quad (2)$$

$$X_c = \sqrt{\frac{n_{\text{eff}}^2 - n_c^2}{n_g^2 - n_{\text{eff}}^2}} \quad (3)$$

and are related by an asymmetry parameter A via

$$X_c = \sqrt{A(X_s^2 + 1) - 1} \quad (4)$$

where A is

$$A = \sqrt{\frac{n_g^2 - n_c^2}{n_g^2 - n_s^2}}. \quad (5)$$

n_{eff} denotes the effective index of the propagating mode which is related to propagation constant of the mode β_m and wavenumber k_0, where $k_0 = 2\pi/\lambda$, by

$$n_{\text{eff}} = \frac{\beta_m}{k_0}. \quad (6)$$

In addition to the normalized waveguide thickness t_{norm}, which is convenient for the generation of normalized design curves, an effective waveguide thickness t_{eff} convenient for the derivation of optimized intensity gradients is defined as follows:

$$(k_0 t_{\text{eff}}) = 2\pi t_{\text{norm}} + \frac{1}{\sqrt{(n_{\text{eff}}^2 - n_s^2)}} + \frac{1}{\sqrt{(n_{\text{eff}}^2 - n_c^2)}}. \quad (7)$$

This effective thickness represents the apparent waveguide thickness, taking into account evanescent field penetration into the substrate and cover.

Since we are considering a purely one-dimensional (1-D) problem, with no variation in the y direction (i.e., $d/dy = 0$), analysis based on a 1-D wave equation is appropriate. By solving Maxwell's equations and applying the appropriate boundary conditions at $x = -t$ and $x = 0$, referring to Fig. 1, an expression for the evanescent field $E_y(x)$ in the cover where $0 \le x \le \infty$, is given for the TE polarization as [32]

$$E_y(x) = C_m\, e^{-q_m x}\, e^{i\varphi} \quad (8)$$

where

$$q_m = \sqrt{\beta_m^2 - n_c^2 k_0^2} \quad (9)$$

is the decay constant in the cover and $\varphi = \beta_m z - \omega t$ represents the phase term. The constant for mth order mode, C_m, is normalized such that it corresponds to a total mode power of 1 W per meter in the y direction and is given as [32]

$$C_m = 2h_m \sqrt{\frac{\omega\mu_0}{|\beta_m|\left(t + \frac{1}{q_m} + \frac{1}{p_m}\right)(h_m^2 + q_m^2)}} \quad (10)$$

where

$$p_m = \sqrt{\beta_m^2 - n_s^2 k_0^2} \quad (11)$$

denotes the decay constant in the substrate,

$$h_m = \sqrt{n_g^2 k_0^2 - \beta_m^2} \quad (12)$$

is the transverse propagation constant in the guide region, ω is the angular frequency and μ_0 is the permeability of free space.The gradient force pulling a nanoparticle onto the waveguide surface results from the exponential decay of the fields into the cover region described in (8). As the evanescent field decays from a maximum on the surface of a waveguide, both intensity and intensity gradient are greatest at the guide-cover interface where $x = 0$. Optimization of a waveguide by carefully selecting the incident wavelength, waveguide thickness and indicies allows one to maximize both the intensity and the intensity gradient at the interface. Knowing the dispersion relation and full expressions for the evanescent fields, expressions for the maximized intensity gradient may be derived, from which optimized waveguide designs result.

B. Derivation of an Optimized Intensity Gradient in the Cover

Using the field expression in (8), the transverse intensity gradient at the interface where $x = 0$, was derived and is given here as

$$\begin{aligned} G_y(x=0) &= \frac{1}{2}\frac{d|E_y(x=0)|^2}{dx} \\ &= -4k_0^2\sqrt{\frac{\mu_0}{\epsilon_0}}P\frac{\sqrt{n_{\text{eff}}^2 - n_c^2}\,(n_g^2 - n_{\text{eff}}^2)}{n_{\text{eff}}(k_0 t_{\text{eff}})\,(n_g^2 - n_c^2)} \end{aligned} \quad (13)$$

where P is the modal power density in W/m and ϵ_0 is the permittivity of free space.

From (13), it is shown that the intensity gradient at the guide-cover interface is explicitly wavelength dependent due to the k_0^2 term which is proportional to λ^{-2}. Hence, in order to obtain a maximized intensity gradient, it is necessary to null the derivative of $G_y(x=0)$ with respect to $2\pi t_{\text{norm}}$, such that

$$\frac{dG_y(x=0)}{d(2\pi t_{\text{norm}})} = 0. \quad (14)$$

By applying

$$\frac{dG_y(x=0)}{d(2\pi t_{\text{norm}})} = \frac{dG_y(x=0)}{d\epsilon_{\text{eff}}}\frac{d\epsilon_{\text{eff}}}{d(2\pi t_{\text{norm}})} = 0 \quad (15)$$

where $\epsilon_{\text{eff}} = n_{\text{eff}}^2$, and using (1) and (13), a normalized transcendental equation is derived, where

$$\left[\tan^{-1} X_s + \tan^{-1} X_c + \frac{1}{X_s} + \frac{1}{X_c} + m\pi\right]\left[\frac{1}{X_c^2} - 3\right] + \frac{1}{X_s^3} + \frac{1}{X_c^3} = 0. \quad (16)$$

This expression which is derived for the first time to our knowledge, is the main result of this paper. Notice that unlike the expression of intensity gradient in (13), the transcendental equation in (16) can be fully written in terms of the normalized thickness t_{norm}, which is evident from the dispersion relation in (1). Hence, the transcendental equation has the advantage of expressing a set of normalized parameters which can be applied to any wavelength desired. The maximized value of intensity gradient at the interface, $G_y(x = 0)$, can be calculated by simply substituting the solutions of optimum t_{norm} and n_{eff} for a set of refractive indexes, obtained from (16), into (13).

By expressing the solutions of the transcendental equation in (16) as X_{s0} and X_{c0}, the optimum condition of $(2\pi t_{\text{norm}})_{\text{opt}}$ in (1) to achieve maximized intensity gradient, can be reexpressed as

$$(2\pi t_{\text{norm}})_{\text{opt}} = \left[\frac{1 + X_{c0}^2}{\text{NA}}\right]^{1/2} \left[\tan^{-1} X_{c0} + \tan^{-1} X_{s0} + m\pi\right] \quad (17)$$

where NA$= \sqrt{n_g^2 - n_s^2}$ is the numerical aperture. Based on (16) and (17), the numerical results showing optimum value of waveguide thickness normalized to wavelength associated with a range of numerical aperture (NA) for three different cover media of water ($n_c = 1.33$), ethylene glycol ($n_c = 1.43$), and a solution of index $n_c = 1.5$ are shown in Fig. 2. The existence of a maximum in the intensity gradient at a waveguide surface is due to the combination of two phenomena. First, as the waveguide thickness is reduced the surface intensity increases until cutoff is approached, when it decreases again. Second, effective index reduces with the waveguide thickness resulting in a reducing exponential decay constant for the evanescent field. For a given power in the mode, the maximum absolute intensity gradient at the surface is found at the optimum thickness given by (17).

Note that, for a particular NA, the optimum t_{norm} decreases with a larger cover index. This can be explained by the fact that as the cover index increases, the field is increasingly drawn into the cover. As a result, the maximized intensity gradient is achieved at a smaller value of t_{norm}. All three curves show a general decrease in optimum t_{norm} with larger NA. This is because, by considering the same total mode power, as the NA increases (i.e., $n_g \gg n_s$), more power is confined in the guide resulting in a smaller wave penetration into the cover and substrate. Consequently, a thinner waveguide or a longer wavelength is required to achieve a maximized intensity gradient in the cover.

For the purpose of comparison in later sections note from Fig. 2 that, for $n_c = 1.33$, the maximized intensity gradient at the interface for NA $= 0.174$ corresponds to an optimum value of $t_{\text{norm}} = 1.7$.

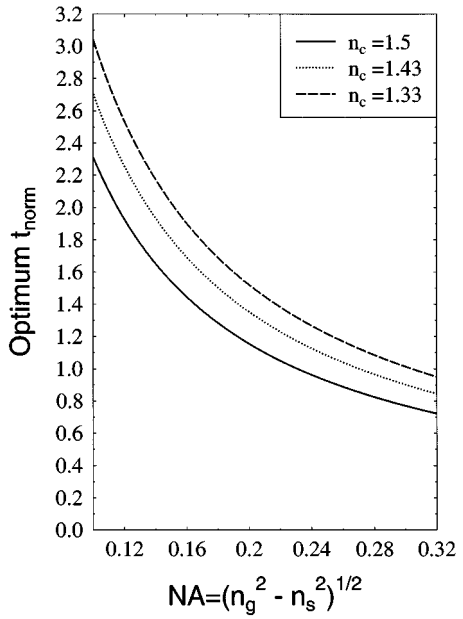

Fig. 2. Design curves for t_{norm}, n_g, and n_s to obtain maximum surface intensity gradient for cover indexes $n_c = 1.33$, 1.43, and 1.5.

C. Intensity Gradient, Evanescent Power, and Surface Intensity for a Specific Case

In this section, the analysis is based specifically on a set of parameters which is most closely associated with K^+–Na^+ ion-exchanged waveguides in soda lime glass substrates with refractive indexes of $n_g = 1.52$ and $n_s = 1.51$, respectively. In this case, the NA $= 0.174$. The cover medium is assumed to be water, which has a refractive index of $n_c = 1.33$. The wavelength dependence of these refractive indexes in real materials is neglected in this analysis. For light to be guided in this asymmetrical waveguide, the condition $1.51 < n_{\text{eff}} < 1.52$ has to be satisfied which results in a corresponding normalized waveguide thickness in the range $1.3 < t_{\text{norm}} < 4.2$ for operation in the single moded region. As n_{eff} approaches the substrate index, n_s, or as t_{norm} becomes close to the cutoff value of approximately 1.3, most of the power is traveling in the substrate. On the other hand, as n_{eff} increases toward the guide index, greater wave penetration into the cover results in a larger value of t_{norm} to satisfy the condition for single-moded operation.

For the given set of indexes, the variation of the surface intensity gradient, total evanescent power, and intensity in the cover region of a waveguide is illustrated in detail, in Section II-C1.

1) Intensity Gradient in the Cover: Based on (13), the variation of the intensity gradient at the interface (where $x = 0$) with normalized thickness for the given set of indexes is shown in Fig. 3. The following features are observed.

1) The intensity gradient has a negative value reflecting the fact that the intensity is decaying away from the interface
2) It is wavelength-dependent and decreases with wavelength as mentioned in Section II-B.
3) Near cutoff, which occurs at $t_{\text{norm}} \approx= 1.3$ for this case, the effective index is close to the substrate index and a very small proportion of the evanescent field penetrates into the cover region, resulting in a small intensity gradient.

4) As $t_{\rm norm}$ increases above cutoff, an increase in field penetration into the cover leads to a rapid increase in intensity gradient as indicated by the steep gradient in Fig. 3.
5) For all wavelengths, the intensity gradient exhibits a maximum at an optimum normalized thickness of approximately 1.7. Hence, for this set of indexes, excellent agreement is found in comparison with the results found using the transcendental equation.
6) Above the optimum value, where the effective index now approaches the guide index, the mode is now increasingly confined in the guide region resulting in a decrease in field penetration into the cover and hence a smaller intensity gradient.

The purpose of optimizing the intensity gradient is to ensure that a nanoparticle is driven by maximum transverse gradient force toward the waveguide. On the other hand, since the forward forces is proportional to the intensity, maximizing the forward forces exerted on a particle would require the maximization of the light intensity in the cover region, which is discussed in Section II-C2).

2) Power and Intensity Distribution in the Cover: From the definition of the integral of the average Poynting vector, the total power per unit waveguide width P_E in the cover can be written as

$$P_E = \frac{\beta_0 P}{4\omega\mu_0 q_0} C_0^2 = \frac{P\left(n_g^2 - n_{\rm eff}^2\right)}{\left(n_g^2 - n_c^2\right)\sqrt{(n_{\rm eff}^2 - n_c^2)}(k_0 t_{\rm eff})} \tag{18}$$

where the subscripts in both C_0 and q_0 correspond to the first order mode, i.e., $m = 0$. In (18), P is 1 W/m while both terms $n_{\rm eff}$ and $(k_0 t_{\rm eff})$ are dependent upon $t_{\rm norm}$, as described by (1) and (7), respectively. The relationship between evanescent power and surface intensity I_0 which is greatest at the guide-cover interface can be written as

$$\begin{aligned} I_0 &= \overline{\vec{S}_z(x=0)} \\ &= \frac{\beta_0 k_0 P}{2\omega\mu_0} C_0^2 \\ &= \frac{2k_0 P\left(n_g^2 - n_{\rm eff}^2\right)}{(k_0 t_{\rm eff})\left(n_g^2 - n_c^2\right)} \\ &= 2k_0\sqrt{n_{\rm eff}^2 - n_c^2} P_E. \end{aligned} \tag{19}$$

The variation of total evanescent power and surface intensity with normalized waveguide thickness $t_{\rm norm}$, as shown in Figs. 4 and 5, respectively, show similar behavior to the intensity gradient. However, by comparing the figures for total evanescent power and surface intensity, one clear distinction can be drawn; unlike the total evanescent power in the cover, P_E, the surface intensity I_0 is explicitly wavelength dependent, due to the presence of the term k_0 in the numerator of (19) which is proportional to λ^{-1}. A point to note from the intensity gradient and intensity plots in Figs. 3 and 5, respectively, is that both exhibit a similar trend with wavelength. Using (19) and (13), the maximum intensity gradient can be expressed in terms of maximum intensity at the interface by

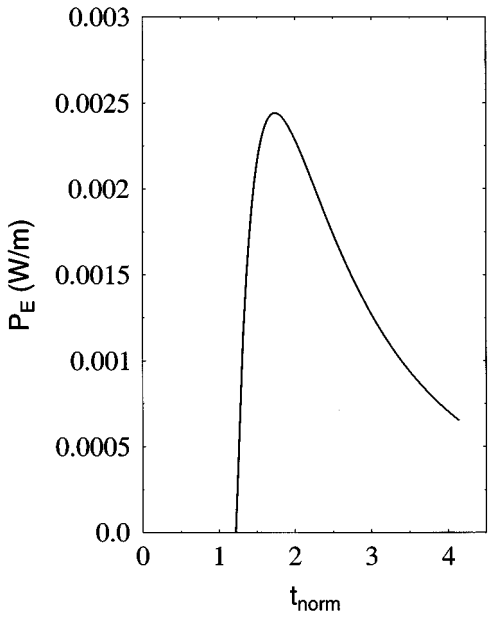

Fig. 3. Intensity gradient at the guide-cover interface $x = 0$ for a given set of indexes: $n_c = 1.33$, $n_g = 1.52$, and $n_s = 1.51$.

$$G_y(x=0) = -2k_0\sqrt{\frac{\mu_0}{\epsilon_0}}\frac{\sqrt{n_{\rm eff}^2 - n_c^2}}{n_{\rm eff}} I_0. \tag{20}$$

Clearly, a proportional relationship between G_y and I_0 exists. This is explained by the fact that, as the total power in the cover region is a constant for a specific normalized thickness, a larger surface intensity at the interface ($x = 0$) will result in a faster decay and hence a stronger gradient. Since G_y and I_0 are maximum at $x = 0$, a particle would experience maximum transverse and forward forces, respectively, at the guide-cover interface.

III. Maximization of Radiation Forces Exerted on a Nanoparticle in the Cover Region

A. Gradient, Dissipative, and Rayleigh Scattering Forces

A second important factor that influences the radiation forces exerted on a Rayleigh sphere is the particle polarizability. Derivation of the forces by extending Maxwell's equation and applying the semiclassical model which is modified to suit the case of a waveguide configuration, and the behavior of the polarizability are addressed in detail in this section.

When a Rayleigh particle is subjected to an applied field, it becomes polarized. A separation of charges, specifically between electrons and nuclei, takes place which results in an induced dipole created in the particle. The force acting on each charge is described by the Lorentz equation which for the case of an electron, is given by [33]

$$\vec{F}_e = -Q\left(\vec{E} + \vec{v}\times\vec{B}\right) - \vec{F}_b \tag{21}$$

and for a nucleus

$$\vec{F}_n = +Q\left(\vec{E} + \vec{v}\times\vec{B}\right) + \vec{F}_b \tag{22}$$

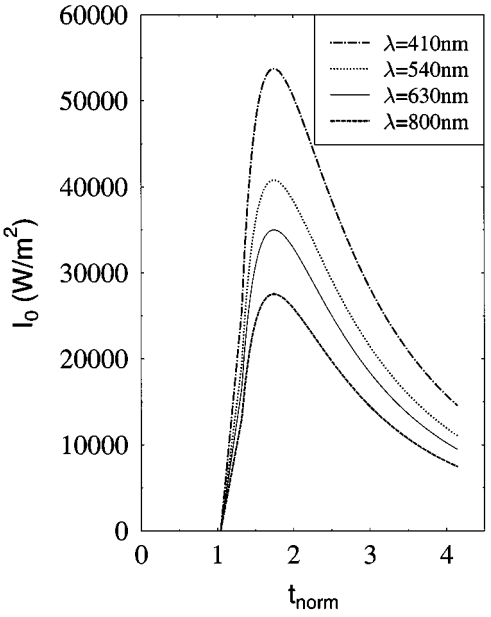

Fig. 4. Total power in the cover region for a given set of indexes: $n_c = 1.33$, $n_g = 1.52$, and $n_s = 1.51$.

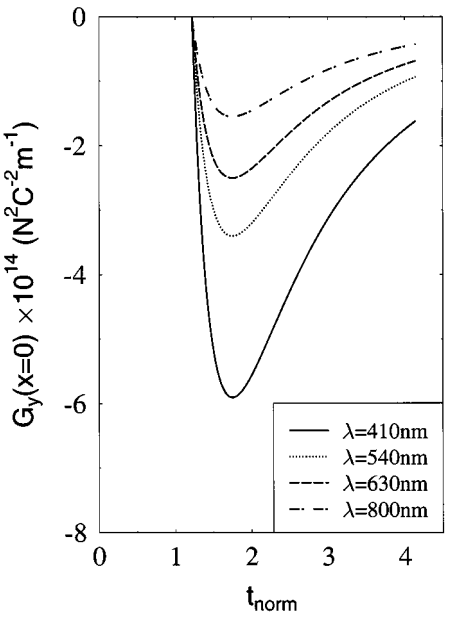

Fig. 5. Intensity at the guide-cover interface $x = 0$ for a given set of indexes: $n_c = 1.33$, $n_g = 1.52$, and $n_s = 1.51$.

where

- Q denotes the elementary charge;
- v the velocity of the charge;
- F_b is the binding force between the opposite charges.

Based on the semiclassical model by Stenholm [33] where the center-of-mass motion is considered, the force, in MKS units, acting on an induced dipole is given as

$$\vec{F}_{e,n} = \left[\vec{\nabla}(\vec{E} + \vec{v} \times \vec{B})\right] \cdot \vec{p} + \frac{d\left(\vec{p} \times \vec{B}\right)}{dt} \tag{23}$$

where the subscript e corresponds to an electron, subscript h corresponds to a nuclei, and $\vec{p}$ is the atomic electric dipole operator. Based on the same assumptions as Stenholm [33], which neglect both the total time derivative of the periodic function $\vec{p} \times \vec{B}$ and the correction term to the electromagnetic force $\vec{v} \times \vec{B}$, the final approximate expression for the force is given as [33], [34]

$$\vec{F}_{e,n} = \left(\vec{\nabla}\vec{E}\right) \cdot \vec{p}. \tag{24}$$

The above dipole operator for a particle, $\vec{p}$, which is dependent on the surrounding medium, applied field and the polarizability of a particle, may be expressed as [25], [35]

$$\vec{p} = \epsilon_0 \epsilon_c \alpha \vec{E} \tag{25}$$

where $\epsilon_c = n_c^2$ is the permittivity of the cover medium. Assuming a complex polarizability

$$\alpha = \alpha' + i\alpha'' = |\alpha| \exp^{i\theta} \tag{26}$$

where

$$\theta = \tan^{-1} \frac{\alpha''}{\alpha'} \tag{27}$$

is the phase in the complex polarizability, we express the time averaged force as shown in (28) at the bottom of the page. Deriving (28) reveals that the average force consists of two main force components; 1) a real part which depends on the spatial variation of the intensity [25], [33], [34]

$$\begin{aligned} \vec{F}_{\text{grad}} &= \tfrac{1}{4}\epsilon_c \epsilon_0 \alpha' \nabla |E(x, y, z)|^2 \\ &= \tfrac{1}{2}\epsilon_c \epsilon_0 \alpha' G_y(x, y, z) \end{aligned} \tag{29}$$

known as the gradient force, as it varies with the gradient of light intensity and 2) an imaginary component relating to the spatial variation in the phase given by

$$\vec{F}_{\text{diss}} = \tfrac{1}{2}\epsilon_c \epsilon_0 \alpha'' |E|^2 \nabla \varphi(x, y, z) \tag{30}$$

known as the dissipative force.

So far we have assumed that attenuation in the propagation direction does not exist. However, for the purpose of investigating the magnitude of the loss required in the waveguide to produce a backward gradient force to counteract the forward force, we assume a decay factor of $e^{-\gamma z}$ in (8) which describes the atten-

$$\overline{\vec{F}_{e,n}} = \overline{\epsilon_0 \epsilon_c \left[(\vec{\nabla}\vec{E}) \cdot \vec{\alpha}\vec{E}\right]} = \overline{\left\{\epsilon_0 \epsilon_c \left[\left(\frac{\partial}{\partial x}\hat{x} + \frac{\partial}{\partial y}\hat{y} + \frac{\partial}{\partial z}\hat{z}\right)\left(\vec{E}_x\hat{x} + \vec{E}_y\hat{y} + \vec{E}_z\hat{z}\right)\right]\right\}} \overline{\left\{|\alpha| e^{i\theta}\left(\vec{E}_x\hat{x} + \vec{E}_y\hat{y} + \vec{E}_z\hat{z}\right)\right\}}. \tag{28}$$

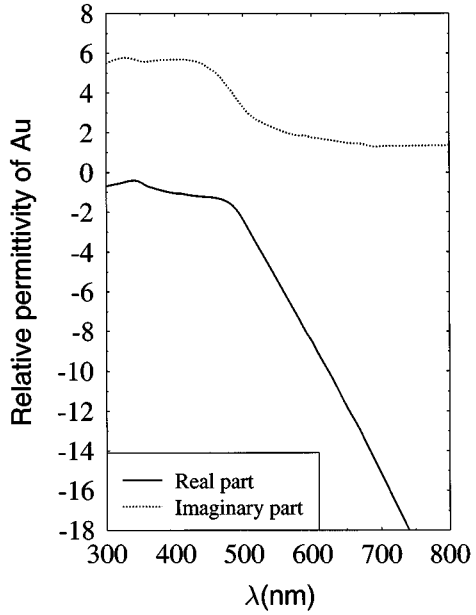

Fig. 6. Relative permittivity of gold.

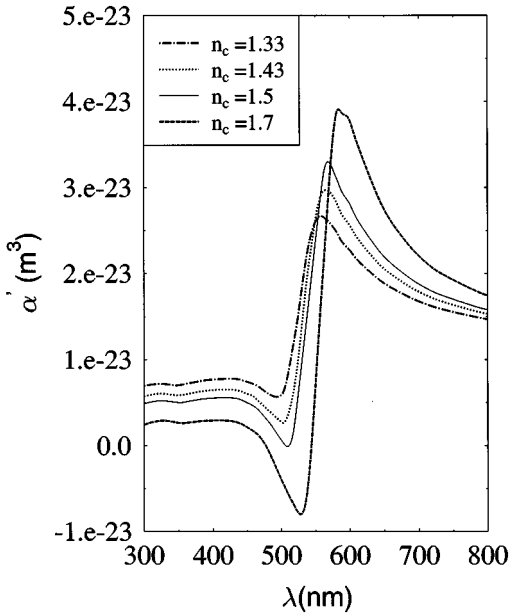

Fig. 7. Real part of polarizability α of a gold sphere versus wavelength for cover indexes $n_c = 1.33, 1.43, 1.5$, and 1.7.

uation of field in the z direction. The damping term γ may be included as the imaginary part of the propagating constant of a mode where $\beta = \beta_0 + i\gamma$. In this analysis, the effect of this loss upon q_0, [see (9)], is not taken into account.

As the evanescent field in the cover is assumed to decay both in the transverse direction and along the direction of wave propagation, using (20) and (29) results in two orthogonal gradient forces, of which the first varies transversely according to

$$\begin{aligned}\vec{F}_{\text{grad},x} &= -\tfrac{1}{2}\epsilon_0\epsilon_c\alpha' q_0|E(x,y,z)|^2\hat{x} \\ &= -\tfrac{1}{2}\epsilon_0\epsilon_c\alpha' q_0 C_0^2 e^{-2q_0x}e^{-2\gamma z}\hat{x} \\ &= -\frac{\epsilon_c}{n_{\text{eff}}c}q_0\alpha' I\hat{x} \end{aligned} \tag{31}$$

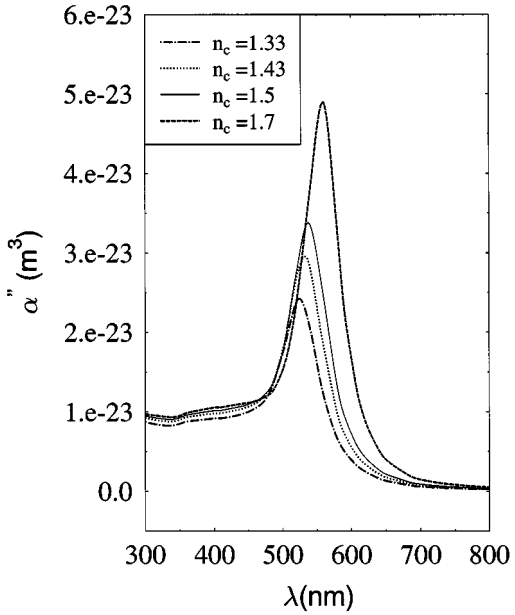

Fig. 8. Imaginary part of polarizability α of a gold sphere versus wavelength for cover indexes $n_c = 1.33, 1.43, 1.5$, and 1.7.

while the second component acts in the $-z$ direction where

$$\begin{aligned}\vec{F}_{\text{grad},z} &= -\tfrac{1}{2}\epsilon_0\epsilon_c\alpha'\gamma|E(x,y,z)|^2\hat{z} \\ &= -\tfrac{1}{2}\epsilon_0\epsilon_c\alpha'\gamma C_0^2 e^{-2q_0x}e^{-2\gamma z}\hat{z} \\ &= -\frac{\epsilon_c}{n_{\text{eff}}c}\gamma\alpha' I\hat{z}. \end{aligned} \tag{32}$$

Based on (8) and (19), the dissipative force in (30) can be solved and is given by

$$\begin{aligned}\vec{F}_{\text{diss},z} &= \tfrac{1}{2}\epsilon_0\epsilon_c\alpha''\beta_0|E|^2\hat{z} \\ &= \tfrac{1}{2}\epsilon_0\epsilon_c\alpha''\beta_0 C_0^2 e^{-2q_0x}e^{-2\gamma z}\hat{z} \\ &= \frac{\epsilon_c}{n_{\text{eff}}c}\beta_0\alpha'' I\hat{z}. \end{aligned} \tag{33}$$

A further contribution to the forces, neglected so far in this analysis due to simplifying assumptions made in deriving (24), is the scattering force, often known as the "light pressure" [36]. This force acts along the direction of wave propagation and may be expressed as [5], [35], [37]

$$\vec{F}_{\text{scat},z} = \frac{n_{\text{eff}}}{c}\beta_0^4\frac{|\alpha|^2}{6\pi}I\,\hat{z} \tag{34}$$

which is proportional to the sixth order of the radius of a sphere.

Note that the presence of n_{eff} in (34) results from considering the effective index of a propagating mode rather than a free-space wave. From (31) to (34), it is clear that all these force components are strongly dependent upon the polarizability of a particle. Hence, in addition to optimizing the waveguide structure, radiation forces can be maximized by maximizing the polarizability of a Rayleigh particle.

B. Polarizability of a Particle

In the electrostatic approximation, the equivalent molecular polarizability of a particle, α, is given as [5]

$$\alpha = 3V\frac{\epsilon - \epsilon_c}{\epsilon + 2\epsilon_c} \tag{35}$$

where $\epsilon = \epsilon' + i\epsilon''$ is the complex permittivity of the particle, which is related to its refractive index via $\epsilon = (n + ik)^2$. The volume of a sphere, given by $V = (4\pi/3)r^3$ may be used, provided that the imaginary part of the index k satisfies the condition $(\lambda/2\pi k) \gg r$; for example, dielectric materials have an imaginary value k close to 0. However, in cases where this condition is not met, correction for the attenuation of the field requires an integral representation of V instead [5], to account for the skin depth.

In the following sections the polarizabilities of dielectric and metallic particles of radius 10 nm in a range of surrounding media will be discussed.

1) Polarizability of a Dielectric Particle: Away from resonances, dielectrics are assumed to be lossless, with refractive index consisting of a dominant real part, which is weakly dependent upon wavelength, and a negligible imaginary part. Latex particles are often used in experimental work and provide a convenient example for calculations and for comparison with metallic nanoparticles. Application of (35) to a latex sphere of index 1.59 and radius 10 nm in surrounding cover media of index 1.33, 1.43, and 1.5, results in a purely real and positive polarizability of 1.57×10^{-24} m^3, 0.92×10^{-24} m^3, and 0.497×10^{-24} m^3, respectively. As α' is positive, the gradient forces in (31) and (32), are expected to move the Rayleigh particle in the negative x and z directions toward the high intensity region.

However, when a dielectric particle has a smaller index than the surrounding medium, the polarizability will be negative causing a positive gradient force to act on the particle which will expel the particle from the high intensity region.

2) Polarizability of a Metallic Particle: In the wavelength range of interest, however, metallic particles are absorbing and have a strongly wavelength dependent complex refractive index which results in a complex polarizability. Experimentally measured values of the relative permittivity of gold [38] are shown in Fig. 6. Based on this data, the wavelength dependent parameters α' and α'' applying to a gold sphere of radius $r = 10$ nm in a range of cover media are illustrated in Figs. 7 and 8, respectively. It is evident from these plots that the polarizability exhibits a strong resonance peak in the visible region. Based on these plots, the peak occurs at $\lambda \approx$550 nm for α' and $\lambda \approx$530 nm for α'', coinciding with the condition in (35) where the denominator of the expression for polarizability approaches zero.

In addition, with an increase in the cover index of the surrounding medium, there is an evident shift in the peak to longer resonant wavelength and an increase in magnitude. Since polarizability and radiation forces as given in (31)–(34), are proportional, the variation in both α' and α'' would affect the way in which these forces vary.

The polarizability of a gold nanoparticle in a surrounding medium of higher refractive index, $n_c = 1.7$, is shown in Figs. 7 and 8, though it should be noted that this cover index would not allow waveguiding in the structure with refractive indexes modeled in Section II-C. Under these circumstances, the real part of the polarizability becomes negative over a narrow wavelength range. This implies that for cover media of high index, the particles may either be drawn into regions of high intensity or expelled from them by tuning the incident wavelength.

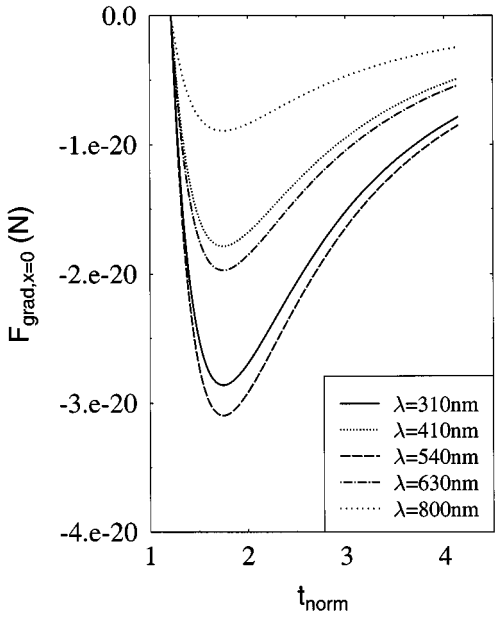

Fig. 9. Transverse gradient force exerted on a gold sphere at the guide-cover interface $x = 0$ for cover index $n_c = 1.33$ versus $t_{\rm norm}$.

On the other hand, α'' remains positive over the entire wavelength range under all conditions. This implies that the dissipative force in (33), whose value depends on α'', is always a positive force in the forward direction.

C. Numerical Results for Forces on Optimized Waveguides

1) Transverse Gradient Force at the Guide-Cover Interface: The transverse gradient force, based on (31) and as shown in Fig. 1 as $F_{\rm grad}$, acts in the direction of the intensity gradient with the maximum force occuring when the intensity gradient is a maximum. We have seen from Section II-C1) that in a waveguide cover, this occurs at the guide-cover interface where $x = 0$. Using (31), the transverse gradient force experienced by a particle in this region, defined in terms of the maximum surface intensity is given as

$$\vec{F}_{\rm grad,\, x=0} = -\frac{\epsilon_c}{n_{\rm eff} c} q_0 \alpha' I_0 \hat{x}. \tag{36}$$

By considering both a gold and a latex sphere of radius $r = 10$ nm, where α' is positive with water as a cover medium (i.e., $n_c = 1.33$), variation in the transverse gradient force at the interface with $t_{\rm norm}$ is shown in Figs. 9 and 11, respectively. Comparing these plots with Fig. 3 shows that these forces vary with $t_{\rm norm}$ in a way similar to the intensity gradient $G_y(x = 0)$ with an optimum value occuring at $t_{\rm norm} = 1.7$. At this waveguide thickness, both the intensity gradient and transverse force at the interface are maximized. Further, the fact that gold particles exhibit resonance in the visible region, while latex particles in the Rayleigh regime do not, is clearly shown by comparing Figs. 10 and 12. Hence, information on both α', which relates to the optical properties of a sphere, and the intensity gradient for a given set of waveguide indexes, are contained in these plots where the influence of both factors on the gradient force is clearly shown. Note also that a gold sphere experiences a force of a magnitude

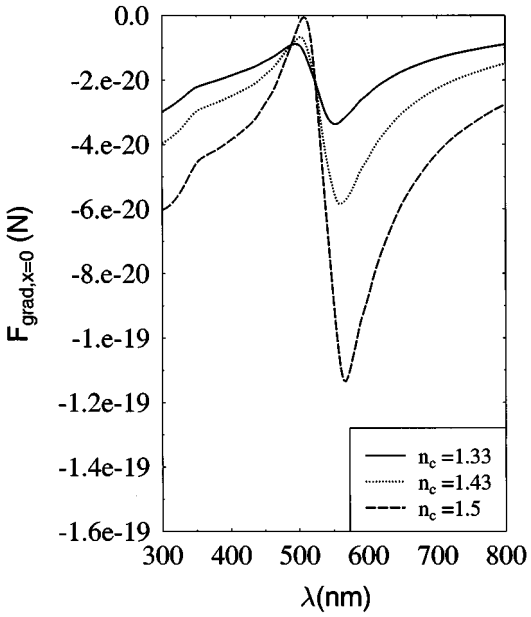

Fig. 10. Transverse gradient force exerted on a gold sphere at the interface at optimum $t_{\rm norm}$ corresponding to each cover indexes $n_c = 1.33, 1.43$, and 1.5 versus wavelength.

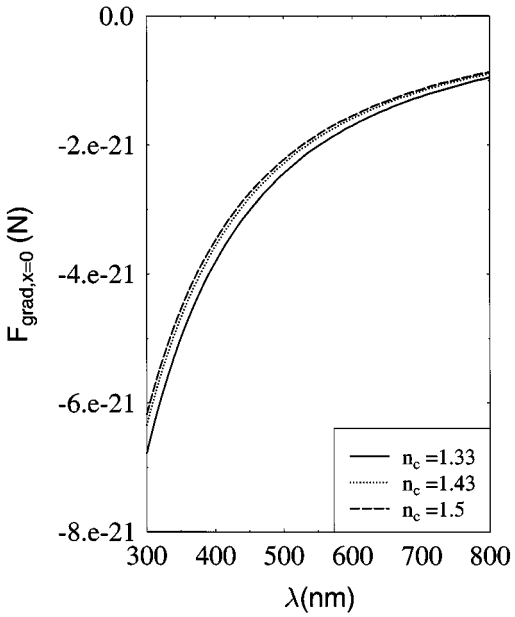

Fig. 12. Transverse gradient force exerted on a latex sphere at the interface at optimum $t_{\rm norm}$ corresponding to each cover indexes $n_c = 1.33, 1.43$, and 1.5 versus wavelength.

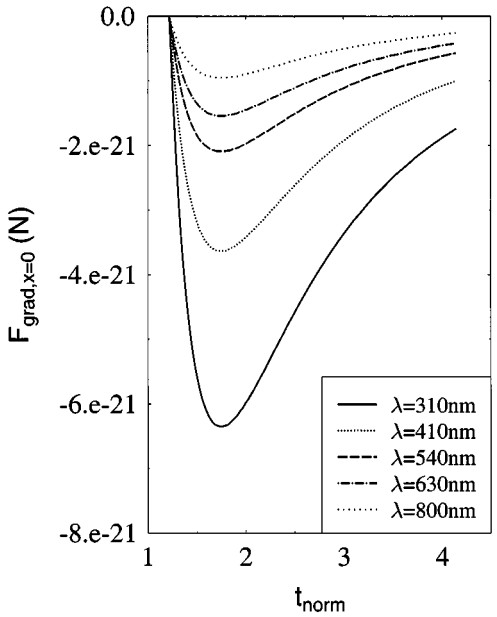

Fig. 11. Transverse gradient force exerted on a latex sphere at the guide-cover interface $x = 0$ for cover index $n_c = 1.33$ versus $t_{\rm norm}$.

approximately ten times larger than that for a latex sphere, due to its greater polarizability as discussed in Section III-B.

At this point, it is clear that one procedure to maximize the gradient force on a particle in the cover is first to select a wavelength which ensures maximum real part of the polarizability. Second, determining the optimum value of the normalized thickness $t_{\rm norm}$, based on the derived transcendental equation as shown in Fig. 3, the corresponding waveguide thickness t for achieving the maximum trapping force can be obtained. Hence, for the particular set of indexes considered, given that the maximum gradient force is achieved at $t_{\rm norm} = 1.7$ and peaks at $\lambda \approx 550$ nm due to particle resonance, the waveguide thickness required for maximization of the force is $t = 935$ nm.

2) Axial Forces at the Guide-Cover Interface: Unlike the gradient force, forward axial forces, primarily the dissipative and Rayleigh scattering forces as denoted by $\vec{F}_{\rm diss}$ and $\vec{F}_{\rm scat}$, respectively, in Fig. 1, exist even in the absence of an intensity gradient. In the cover region, these forces act in the forward wave propagating direction and are greatest at the guide-cover interface (i.e., $x = 0$, $z = 0$) where maximum intensity occurs. For axial trapping to occur, the existence of a backward axial force is required to balance the forces in the forward direction. The backward force due to waveguide losses, given as $\vec{F}_{{\rm grad},\, z}$ in (32), is found to be negligibly small for practical values of loss and is therefore neglected here. However, superposition of additional waves propagating in different directions may allow stable trapping to be achieved on waveguide surfaces [2].

From (33) and (34), the forward dissipative and scattering forces exerted on a particle located at $z = 0$ on the guide-cover interface are given as

$$\vec{F}_{{\rm diss},\, z=0} = \frac{\epsilon_c}{n_{\rm eff} c}\beta_0 \alpha'' I_0 \hat{z}. \tag{37}$$

$$\vec{F}_{{\rm scat},\, z=0} = \frac{n_{\rm eff}}{c}\beta_0^4 \frac{|\alpha|^2}{6\pi} I_0 \hat{z}. \tag{38}$$

The maximum forward forces at the interface exerted on a gold sphere are shown against normalized thickness in Fig. 13 for the Rayleigh scattering force and Fig. 14 for the dissipative force. The magnitude of the scattering force is approximately 100 times smaller than the dissipative force. On the other hand, for the case of latex spheres, which are assumed lossless so that $\alpha'' = 0$, the only forward force acting on them is the scattering force component which is shown in Fig. 15.

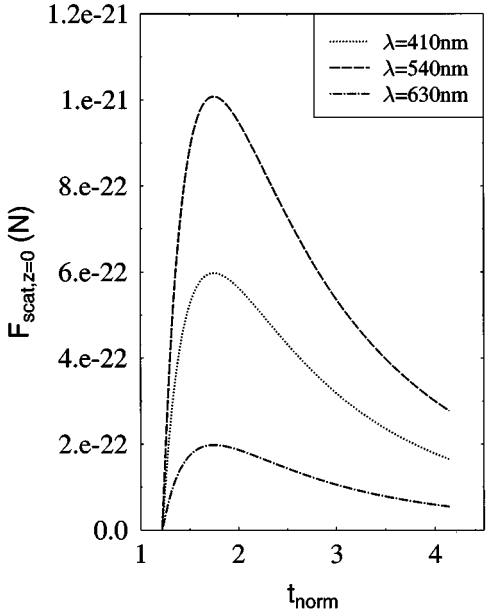

Fig. 13. Scattering force exerted on a gold sphere at the guide-cover interface for cover index $n_c = 1.33$ versus $t_{\rm norm}$.

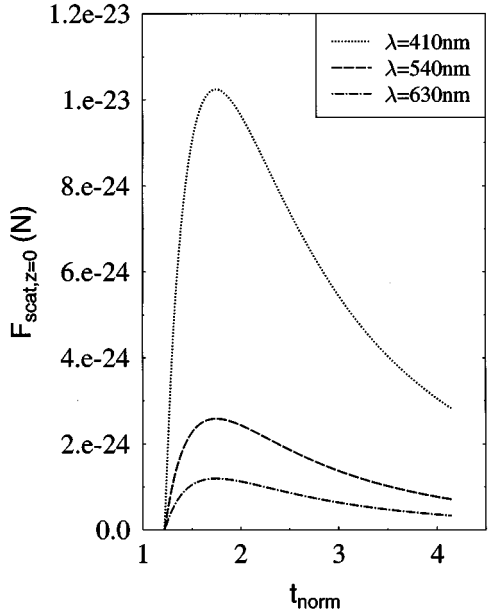

Fig. 15. Scattering force exerted on a latex sphere at the guide-cover interface for cover index $n_c = 1.33$ versus $t_{\rm norm}$.

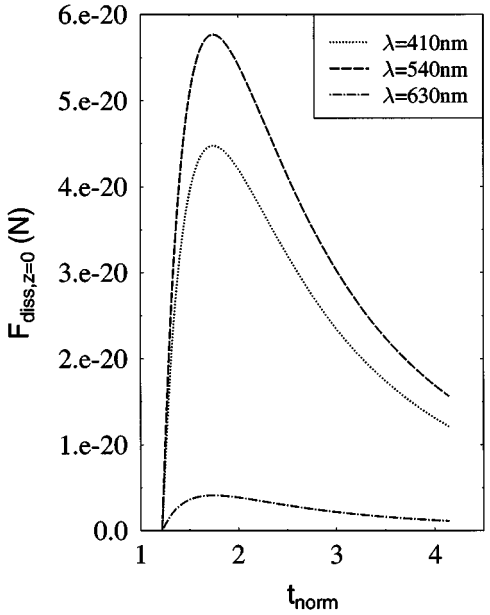

Fig. 14. Dissipative force exerted on a gold sphere at the guide-cover interface for cover index $n_c = 1.33$ versus $t_{\rm norm}$.

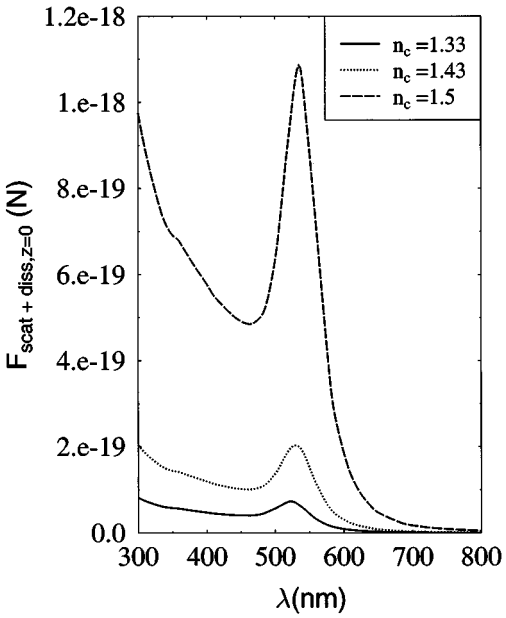

Fig. 16. Sum of scattering and dissipative force exerted on a gold sphere at the guide-cover interface at optimum $t_{\rm norm}$ corresponding to each cover indexes $n_c = 1.33$, 1.43, and 1.5.

3) Discussion: Integrated optical waveguides may be used for trapping and propelling nanoparticles and potentially for simultaneous measurement of their optical properties. Colloidal gold nanoparticles of radius of order 10 nm are of particular interest for studies of surface enhanced Raman spectra (SERS) of species attached at their surfaces. Compared with conventional focused beam optical traps, gradient forces tend to be weaker for a given input power because the substantially reduced peak intensity in the evanescent field and because the spotsize is generally larger than the spotsize of a focused Gaussian beam, especially if the waveguide is designed to connect efficiently to optical fiber. As the duration for which a particle stays trapped depends strongly upon the gradient force, it is important to be able to design waveguides for maximum trapping force per unit power. In Section II we developed a transcendental equation which enables straightforward optimization of the intensity gradient in the evanescent field of a planar optical waveguide and in Section III we gave numerical examples of the trapping forces on 10-nm particles in this evanescent field normalized to modal power per unit width of such an optimized waveguide. These results may be useful viewed in the light of published results for the maximum gradient force on a gold nanoparticle in a focused Gaussian trap. Reference [4] gives this force on an 18 nm gold sphere in water in a Gaussian

beam focused to a beam radius of 0.5 μm at a wavelength of 1047 nm to be 5.8×10^{-4} pN/mW; this resulted in an average nanoparticle escape time of 5 s. Assuming that a channel waveguide is realized with a lateral spotsize of 6 μm, typical of potassium ion-exchanged waveguides, our results in Fig. 10 show that a gold sphere of the same size would experience a gradient force of approximately 10^{-4} pN/mW in water for the optimized waveguide at the optimum wavelength. In another example, gold Mie particles of radius 250 nm have been shown to move forward along an unspecified channel waveguide carrying a modal power of order 80 mW at 1047 nm at a velocity greater than 5 μm/s [12]. Our calculations based on Fig. 16, for an optimized waveguide with a lateral spotsize of 6 μm at this wavelength show that a 40-nm radius gold sphere would be propelled forward at a velocity, given by Navier–Stokes law, of 1 μm/s for a modal power of 125 mW. This velocity would tend to increase with the square of the particle radius, due to the finite skin depth of the particle. The use of a wavelength close to the particle resonance at approximately 550 nm would lead to a velocity of 1 μm/s for a reduced modal power of 0.3 mW. The forward forces are expected to be useful for positioning particles at a surface but stable trapping may be achieved by establishing a standing wave in the waveguide to counteract the forward forces and set up periodic gradient force traps along the direction of the waveguide [12]. The use of optimized waveguide designs at the wavelength of particle resonance is expected to lead to stable traps where the intensity of Raman spectra generated at the surface of the particle is also optimized.

Comparison of the forces on metallic nanoparticles with those on latex spheres is useful to illustrate differences in their behavior. The variation of the total forward forces at the interface with wavelength at optimum t_{norm}, corresponding to each particular set of indexes, as shown in Fig. 16 for gold and Fig. 17 for latex, clearly reflects the wavelength dependency of I_0 and of the polarizability. In the case where water is the surrounding medium ($n_c = 1.33$), the total forward force exerted on a gold sphere as shown in Fig. 16 exhibits a resonant peak at a wavelength close to $\lambda = 530$ nm. Since $F_{\mathrm{diss}} \propto \alpha''$ where the latter peaks at exactly the same wavelength (refer to Section III-B2 and Fig. 8), the dominance of F_{diss} over F_{scat} in the total forward force is clearly shown.

Some other interesting points are worth noting. First, the forward force on a Rayleigh gold sphere, exceeds that of a latex sphere where

$$\frac{\vec{F}_{\mathrm{scat+diss},\, x=0,\, \mathrm{gold}}}{\vec{F}_{\mathrm{scat},\, x=0,\, \mathrm{latex}}} \approx 10^5. \tag{39}$$

This can be explained by the smaller polarizability and absence of the dissipative force component for a latex sphere. Hence, a gold sphere is expected to be propelled forward in the $+z$ direction at a velocity much greater than a latex sphere. Second, by comparing the maximum gradient and forward forces, we find that in the case of a gold sphere,

$$\vec{F}_{\mathrm{grad},\, x=0} \approx \vec{F}_{\mathrm{scat+diss},\, x=0} \tag{40}$$

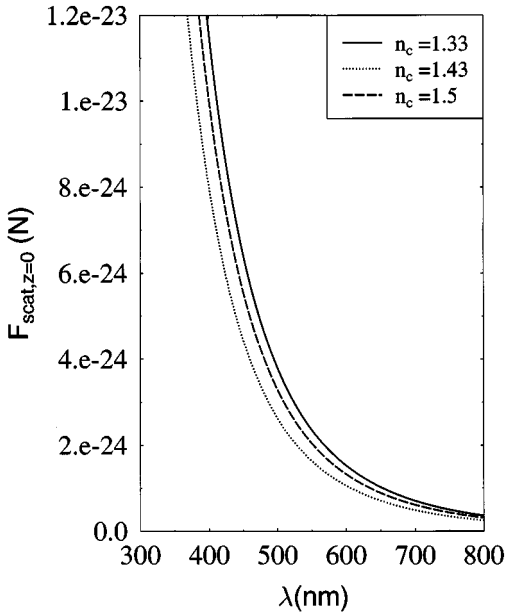

Fig. 17. Scattering force exerted on a latex sphere at the guide-cover interface at optimum t_{norm} corresponding to each cover indexes $n_c = 1.33$, 1.43, and 1.5.

while for the case of a latex sphere,

$$\vec{F}_{\mathrm{grad},\, x=0} \gg \vec{F}_{\mathrm{scat+diss},\, x=0}. \tag{41}$$

For instance, at $\lambda = 530$ nm, the gradient force exerted on a latex sphere is 2×10^{-21} N as compared to 2×10^{-24} N for the forward force, a difference in magnitude of 10^3. Therefore, wheareas a gold sphere is driven by equally strong transverse and axial forces, a latex sphere experiences a forward force which is insignificant compared to the gradient force acting on it. Finally, as the plots for forward force suggest a maximum at $t_{\mathrm{norm}} = 1.7$ and a peak at $\lambda = 530$ nm for a Rayleigh gold sphere, an optimized forward force is exerted on it at a corresponding waveguide thickness of 901 nm. This is slightly smaller than the thickness required for optimizing the gradient force, described in Section III-C1.

IV. Conclusion

Movement and trapping of nanoparticles in the evanescent field of optical waveguides is of potential interest for particle sorting and mixing and for the optical interrogation of trapped particles at surfaces. These applications require a thorough understanding of the interactions of particles with the evanescent field of a waveguide. In this paper we have presented a detailed study which quantifies the various forces acting upon dielectric and metallic particles in the cover region of a homogeneous planar waveguide, in the case of the TE polarization, for the first time. The particles are drawn toward or repelled from the surface of the waveguide by a gradient force whose direction and magnitude depends upon the real part of the polarizability of the particle and the intensity gradient in the evanescent field. The particles also experience a force in the direction of modal propagation due to the sum of dissipative and scattering forces. A minor gradient force contribution in this direction, due to waveguide losses, was found to be negligible for

practical cases. The total power in the cover region and the surface intensity at the guide-cover interface in a planar waveguide were studied in terms of a normalized waveguide thickness, and a transcendental equation has been derived which allows optimization of the waveguide using simple normalized design curves, as shown in Fig. 2, yielding a maximum intensity gradient at the guide-cover interface. Numerical results are given for a specific set of waveguide indexes, and the normalized waveguide thickness at which the maximum intensity gradient occurs agrees well with that determined using the transcendental equation. For the set of indexes considered, where the guide, substrate and cover indexes are $n_g = 1.52$, $n_s = 1.51$, and $n_c = 1.33$, respectively, the optimum normalized waveguide thickness is found to be approximately 1.7. The polarizabilities of latex and gold nanoparticles in a range of surrounding media are given and the gradient, dissipative, and scattering forces upon these at the surface of a waveguide are described. Numerical results for each of these force components are presented in each case for the waveguide parameters described previously and, finally, the resultant transverse and forward forces on these nanoparticles on optimized waveguides are shown as a function of wavelength, allowing the wavelength and waveguide design to be selected.

ACKNOWLEDGMENT

The authors would like to thank Dr. R. D. Harris, and colleagues at the University of Tübingen, for the data in Fig. 6.

REFERENCES

[1] A. Ashkin, "Acceleration and trapping of particles by radiation pressure," *Phys. Rev. Lett.*, vol. 24, pp. 156–159, Jan. 1970.
[2] ——, "Optical levitation by radiation pressure," *Appl. Phys. Lett.*, vol. 19, pp. 283–285, Oct. 1971.
[3] ——, "Trapping of atoms by resonance radiation pressure," *Phys. Rev. Lett.*, vol. 40, pp. 729–732, Mar. 1978.
[4] A. Ashkin, J. M. Dziedzic, J. E. Bjorkholm, and S. Chu, "Observation of a single-beam gradient force optical trap for dielectric particles," *Opt. Lett.*, vol. 11, pp. 288–290, May 1986.
[5] K. Svoboda and S. M. Block, "Optical trapping of Rayleigh metallic particles," *Opt. Lett.*, vol. 19, pp. 930–932, July 1994.
[6] R. Omori, T. Kobayashi, and S. Suzuki, "Observation of a single-beam gradient-force optical trap for dielectric particles in air," *Opt. Lett.*, vol. 22, pp. 816–818, June 1997.
[7] A. Ashkin, "Forces of a single beam gradient laser trap on a dielectric sphere in the ray optics regime," *Biophys. J.*, vol. 61, pp. 569–582, Feb. 1992.
[8] M. Padgett and L. Allen, "Optical tweezers and spanners," *Phys. World*, vol. 10, pp. 35–38, June 1997.
[9] R. J. Cook and R. K. Hall, "An electromagnetic mirror for neutral atoms," *Opt. Commun.*, vol. 43, pp. 258–260, May 1980.
[10] V. I. Balykin and V. S. Letokhov, "Laser optics of neutral atomic beams," *Phys. Today*, vol. 40, pp. 23–28, Apr. 1989.
[11] S. Kawata and T. Sugiura, "Movement of micrometer-sized particles in the evanescent field of a laser beam," *Opt. Lett.*, vol. 17, pp. 772–774, June 1992.
[12] S. Kawata and T. Tani, "Optically driven Mie particles in an evanescent field along a channeled waveguide," *Opt. Lett.*, vol. 21, pp. 1768–1770, Nov. 1996.
[13] L. Novotny, R. X. Bian, and X. S. Xie, "Theory of nanometric optical tweezers," *Phys. Rev. Lett.*, vol. 79, pp. 645–648, July 1997.
[14] K. Taguchi, H. Ueno, H. Matsuzaki, and M. Ikeda, "Optical manipulation and observation of nonlinear phenomena from optically trapped microscopic object using optical fibers," in *Proc. OECC Tech. Dig.*, July 1998, pp. 68–69.
[15] A. Ashkin, J. M. Dziedzic, and T. Yamane, "Optical trapping and manipulation of single cells using infrared beams," *Nature*, vol. 330, pp. 769–771, Dec. 1987.
[16] T. Buican, M. J. Smith, H. A. Crissman, G. C. Salzman, C. C. Stewart, and J. C. Martin, "Automated single-cell manipulation and sorting by light trapping," *Appl. Opt.*, vol. 26, pp. 5311–5316, Dec. 1987.
[17] A. Ashkin and J. M. Dziedzic, "Optical trapping and manipulation of viruses and bacteria," *Nature*, vol. 235, pp. 1517–1520, Mar. 1987.
[18] A. Ashkin, "Application of laser radiation pressure," *Science*, vol. 210, pp. 1081–1088, Dec. 1980.
[19] S. Kawata, Y. Inouye, and T. Sugiura, "Near-field scanning optical microscope with a laser trapped probe," *Jpn. J. Appl. Phys.*, vol. 33, pp. L1725–L1727, June 1994.
[20] M. Gu and P. C. Ke, "Image enhancement in near-field scanning optical microscopy with laser trapped metallic particles," *Opt. Lett.*, vol. 24, pp. 74–76, Jan. 1999.
[21] R. Gussgard, T. Lindmo, and I. Brevik, "Calculation of the trapping force in a strongly focused laser beam," *J. Opt. Soc. Amer. B*, vol. 9, pp. 1922–1930, Oct. 1992.
[22] J. P. Barton, D. R. Alexander, and S. A. Schaub, "Internal and near-surface electromagnetic fields for a spherical particle irradiated by a focused laser beam," *J. Appl. Phys.*, vol. 64, p. 1632, 1988.
[23] ——, "Internal fields of a spherical particle illuminated by a tightly focused laser beam," *J. Appl. Phys.*, vol. 65, p. 2900, 1989.
[24] E. Almaas and I. Brevik, "Radiation forces on a micrometer-sized sphere in an evanescent field," *J. Opt. Soc. Amer. B*, vol. 12, pp. 2429–2438, Dec. 1995.
[25] P. Zemanek, A. Jonas, L. Sramek, and M. Liska, "Optical trapping of Rayleigh particles using a Gaussian standing wave," *Opt. Commun.*, vol. 151, pp. 273–285, June 1998.
[26] Y. Harada and T. Asakura, "Radiation forces on a dielectric sphere in the Rayleigh scattering regime," *Opt. Commun.*, vol. 124, pp. 529–541, Mar. 1996.
[27] F. Depasse and D. Courjon, "Inductive forces generated by evanescent light fields: Application to local probe microscopy," *Opt. Commun.*, vol. 87, pp. 79–83, Jan. 1992.
[28] M. Quinten, A. Pack, and R. Wannemacher, "Scattering and extinction of evanescent waves by small particles," *Appl. Phys. B*, vol. 68, pp. 87–92, July 1999.
[29] K. Ajito, "Combined near-infrared Raman microprobe and laser trapping system: Application to the analysis of a single organic microdroplet in water," *Appl. Spec.*, vol. 52, pp. 339–342, 1998.
[30] O. Parriaux and P. Dierauer, "Normalized expressions for the optical sensitivity of evanescent wave sensors," *Opt. Lett.*, vol. 19, pp. 508–510, Apr. 1994.
[31] O. Parriaux and G. J. Veldhuis, "Normalized analysis for the sensitivity optimization of integrated optical evanescent-wave sensors," *J. Lightwave Technol.*, vol. 16, pp. 573–582, Apr. 1998.
[32] A. Yariv, *Quantum Electronics*. New York: Wiley, 1989, pp. 600–606.
[33] S. Stenholm, "The semiclassical theory of laser cooling," *Rev. Mod. Phys.*, vol. 58, pp. 699–739, July 1986.
[34] S. Stenholm, "Light forces put a handle on the atom: To cool and trap atoms by laser light," *Contemp. Phys.*, vol. 29, pp. 105–123, 1988.
[35] M. Kerker, *The Scattering of Light and Other Electromagnetic Radiation*. New York: Academic, 1969, pp. 32–37.
[36] D. W. Pohl *et al.*, *Forces in Scanning Probes Methods*, H. J. Guntherodt *et al.*, Eds., June 1997, vol. 22, pp. 235–248.
[37] J. D. Jackson, *Classical Electrodynamics*. New York: Wiley, 1975, pp. 413–414.
[38] R. D. Harris, "Waveguide surface plasmon resonance biosensor," Ph.D. dissertation, Optoelectronics Research Centre, Univ. of Southampton, U.K., Feb. 1996.

L. N. Ng was born in Cambridge, U.K., in 1973. She received the B.Eng. degree in electronics engineering in 1966. She is currently working towards the Ph.D. degree at Optoelectronics Research Centre in the University of Southampton, U.K., dealing with the trapping and manipulation of nanoparticles on wavelength surfaces.

B. J. Luff received the D.Phil. degree in physics from the University of Sussex, U.K., in 1990.

He has since worked at Sussex on luminescence spectroscopy of optoelectronic materials and at the Optoelectronics Research Centre at the University of Southampton, U.K., on the development of integrated optical devices. He is currently Manager of the Component Development Group at Bookman Technology, Oxfordshire, U.K.

M. N. Zervas (M'88) was born in Dimaina-Nafplias, Greece, in 1959. He received the Diploma degree in electrical engineering from Aristotle University of Thessaloniki, Greece, in 1983, the M.Sc. degree (with distinction) in applied and modern optics from the University of Reading, U.K., in 1985, and the Ph.D. degree in fiber optics from the University College London, U.K., in 1989.

During his postgraduate studies, he was awarded scholarships from the State Scholarships Foundation of Greece (IKY) and the Bodossakis Foundation, Athens, Greece. In 1990, he was appointed Lecturer in the Faculty of Electrical Engineering, University of Thessaloniki. In 1991, he joined the Optoelectronics Research Centre (ORC), University of Southampton as a Research Fellow. In 1995, he was appointed Research Lecturer in the ORC and Electronics and Computer Science Department (ECS), University of Southampton. In 1999, he was appointed Professor in Optical Communications within the ORC. His main research interests are in the areas of erbium-doped fiber amplifiers, dispersion compensation, fiber and waveguide gratings, distributed feedback fiber lasers, WDM devices, surface-plasmon-polaritons, and optical trapping. He is the author and coauthor of over 110 technical publications and 15 patents.

Dr. Zervas has served as a member of program committees of various international conferences. He was the general Co-Chair at the 1999 Optical Amplifiers Meeting and Their Applications. In 1996, he shared a prize on "Metrology for World Class Manufacturing Awards" for his contribution on the development of a high-accuracy fiber grating characterization system.

J. S. Wilkinson received the B.Sc.Eng. degree in electronics and the Ph.D. degree in integrated optics from the University College London, U.K., in 1977 and 1985, respectively.

From 1977 to 1979, he was with the GEC Hirst Research Centre working on optical fiber telecommunications systems. From 1983 to 1985, he was with the Department of Nephrology of St. Bartholomew's Hospital, London, U.K., working on sensing and control for hemodialysis procedures. He is now Reader in optoelectronics in the Department of Electronics and Computer Science, University of Southampton, U.K. He is also affiliated with the Optoelectronics Research Centre at Southampton University, where he leads the Integrated Optics and Microstructures Group investigating integrated optical devices including chemical and biochemical sensors with particular application to water quality monitoring, passive devices for telecommunications, and waveguide lasers and amplifiers.